
Article:
Bárcena-González, G., Guerrero-Lebrero, M. P., Guerrero, E. et al. (5 more authors) (2019) HAADF-STEM Image Resolution Enhancement Using High-Quality Image Reconstruction Techniques: Case of the Fe3O4(111) Surface. Microscopy and Microanalysis. ISSN: 1431-9276

https://doi.org/10.1017/S1431927619014788

HAADF-STEM image resolution enhancement using High-Quality Image Reconstruction Techniques: case of Fe_3O_4(111) surface

G. Bárcena-González[1], M. P. Guerrero-Lebrero[1], E. Guerrero[1], A.Yañez[1], B. Nuñez-Moraleda[1], D. Kepaptsoglou [2,3], V. K. Lazarov[2] and P. L. Galindo[1]

[1]Department of Computer Science and Engineering, Universidad de Cádiz, 11510 Puerto Real, Spain

[2]Department of Physics, University of York, Heslington, York, United Kingdom

[3]SuperSTEM Laboratory, SciTech Daresbury Campus, Daresbury WA4 4AD, United Kingdom

Corresponding author: guillermo.barcena@uca.es

From simple averaging to more sophisticated registration and restoration strategies, such as Super-resolution (SR), there exist different computational techniques that use series of images of the same object to generate enhanced images where noise and other distortions has been reduced. In this work we provide qualitative and quantitative measurements of this enhancement for high angle annular dark field (HAADF) scanning transmission electron microscopy imaging (STEM). These images are compared in two ways, qualitatively through visual inspection in real and reciprocal space, and quantitatively, through the calculation of objective measurements, such as signal-to-noise ratio (SNR) and atom column roundness. Results show that these techniques improve the quality of the images. In this paper we use a SR methodology that allows to take advantage of the information present in the image frames and to reliably facilitate the analysis of more difficult region of interest in an experimental image, such as surfaces and interfaces. By acquiring a series of cross-sectional experimental images of magnetite (Fe_3O_4) thin films (111), we have generated interpolated images using averaging and

SR and reconstruct the atomic structure of the very top surface layer that consist of full monolayer of Fe, with topmost Fe atoms in tetrahedrally coordinated site.

Keywords: Drift distortion, Image disturbances, Scan noise, Alignment, Reconstruction, HAADF images

1. Introduction

High Angle Annular Dark Field Scanning Transmission Electron Microscopy (HAADF-STEM) has demonstrated remarkable results for analysing the composition and structure of nano-objects, reaching sub-Å resolution in aberration-corrected microscopes. Nevertheless, during the image acquisition process and due to environmental perturbations, such as airflow, acoustic noise, floor vibrations, AC and DC magnetic fields, temperature fluctuations etc., the acquired images usually contain pixel values that is not directly related to the scattering of the real atomic columns (Jones et al., 2015; Jones & Nellist, 2013). Thus the image sharpness is disturbed generating an added difficulty for analysis. In the last decade, an increasing number of works have appeared addressing this problem. They are based mainly on maximum entropy and deconvolution processing (Nakanishi et al., 2002; Watanabe et al., 2002) or reciprocal space approaches (N Braidy, Le Bouar, Lazar, & Ricolleau, 2012; Nadi Braidy, Le Bouar, Lazar, & Ricolleau, 2012; Jones & Nellist, 2013). As microscopes can now provide multiple images of the same sample region in a very short period of time, methods that rely on the use of series of images are being developed. Instead of using a single image to extract information, the underlying idea is to take advantage of the entire series of images to reduce scan noise, drift distortion and other artefacts, and to ultimately improve resolution.

One of the most straightforward approaches that falls into this category is averaging the series of images, such processing involves basic arithmetic operations between images and is

computationally simple and fast. More advanced techniques such as IMAGE-WARP (Rečnik, Möbus, & Šturm, 2005), RevSTEM (Sang & LeBeau, 2014) (rotating the scan coordinate system between successive frames of a series of LR images), STEM-SI Warp (Wang et al., 2018) (correcting the distortions using prior knowledge of the crystal structure) or using two images without prior image features (Ophus, Ciston, & Nelson, 2016) have demonstrated to be efficient, although they require either to obtain the atomic model as reference or varying the scan angle to obtain the series of images. Other approaches apply registration or restoration algorithms to obtain an image from the series with the same pixel density as the original one (Benjamin Berkels et al., 2014; Binev et al., 2012; Kimoto et al., 2010; Mevenkamp et al., 2015; Saito et al., 2009; Yankovich, Berkels, Dahmen, Binev, & Voyles, 2015).

All these methods do not generate a final image with more resolving power, that is, the image resulting from sampling and interpolating a sequence of images does not have greater sharpness, but often larger number of pixels. Therefore, the interpolated image does not contain more details than its original and resolution remains the same. The resolving power of an image can be increased by adding high-frequency information typically based on knowledge about the specific image model.

A higher resolving power is also obtained when the aliasing ambiguity in an image can be removed, which can be achieved by Super Resolution (SR) techniques. SR allows the generation of a higher resolution (HR) image from several noisy/not well enough sampled frames (or Low Resolution, LR, images) from the same object or scene (Kang & Chaudhuri, 2003; Yang & Huang, 2010). Thus, SR removes the aliasing ambiguity by incorporating additional information obtained from LR series. In the field of strain analysis we have already studied how the precision of the strain analysis can be enhanced when SR methodologies are applied to experimental images (Bárcena-González et al., 2016). In a previous paper (Bárcena-González et al., 2017) we reviewed the main registration and restoration algorithms, analysing

their performance when they are applied to the field of microscopy using simulated images, and a complete methodology of Super Resolution was presented. A current trend is based on non-rigid approximations in the registration stage, however in our study we aimed at reaching similar accuracy but addressing the most complex calculations in the reconstruction stage using rigid registration. We demonstrated that with a small number of experimental images resolution could be enhanced while distortions minimized, providing a more detailed and realistic high quality image than any individual image from the series

In this work we have used experimental series of Magnetite (Fe_3O_4) cross-sectional HAADF-STEM images. Averaging, which generates images of the same size as the originals, were compared against SR, whose larger size HR images are expected to provide better resolving power. First a qualitatively evaluation in the real space and reciprocal space is carried out. Fourier Transform is used since it helps to identify false spots as an evidence of periodic distortions or noise, as well as to observe additional Fourier spots more clearly when the image has a good quality. Then, different objective quality measurements are provided, such as such as signal-to-noise ratio (SNR) and different metrics of atom column roundness to quantify the resolving power of the generated images against the experimental micrographs. The main idea is to keep many low electron dose images at a minimum allowable spatial resolution and the overall cumulative electron dose as low as possible with an acceptable level of physical resolution. We demonstrate that the use of these techniques can reliably facilitate the analysis of image areas where resolution is critical to uniquely identified materials structure, e.g. at surfaces and interfaces.

2. Materials and methods

The overall SR process comprises two main steps: alignment and reconstruction (Nakanishi et al., 2002; Watanabe et al., 2002). A wide variety of methods to obtain a robust and efficient SR

methodology have been proposed (Nasrollahi & Moeslund, 2014), but due to the particular features of HAADF-STEM images (specimen drift, scanning errors), its direct application may perform poorly. During scanning, electromagnetic, mechanical or acoustic perturbations can cause some movements in the sample. Image alignment stage (see Fig 1.a) calculates the displacement and rotation of each LR image with respect to a reference one, according to the coplanarity hypothesis, which assumes that shift and rotation are parallel to the image plane. Vandewalle's algorithm (Vandewalle, Süsstrunk, & Vetterll, 2006) has been selected in this work to calculate the rotation angle between two images. To obtain the displacement parameter, we first apply a low-pass filtering to the series and then normalized cross-correlation between each frame and the image selected as reference. We have implemented an iterative procedure to determine the reference image that reduces the global drift in the series and provides the most accurate values for registration (Bárcena-González et al., 2017). Before reconstruction, in order to increase the pixel density, we apply a 2x upsampling using bicubic interpolation (see Fig 1.b). The reconstruction stage (see Fig 1.c) combines information from the series to obtain an image with more definition and quality. Buades (Buades, Coll, & Morel, 2005) proposed the NonLocal Means (NLM) denoising algorithm. The NLM algorithm assumes that the content of an image is likely to repeat itself within some neighbourhood and calculates a weighted averaging on those pixels in the same patch (search window) whose intensity distributions are close to each other, in terms of the Euclidean distance. Protter (Protter, Elad, Member, Takeda, & Member, 2009) adapted this method to SR, showing a very robust performance in registration and motion tracking, as well as using electron microscopy images (Binev et al., 2012)(Mevenkamp et al., 2015)(Yankovich et al., 2015)(B. Berkels et al., 2012). The NLM algorithm is governed by three parameters, namely the weight-decay control parameter to manage the amount of noise to be taken into account in the final image, the radius of the neighbourhood, to find the similarity between two pixels and the radius of a search window,

which is centred at the current pixel being computed.

We consider a sample of Fe_3O_4(111) thin film to acquire a series of 10 HAADF-STEM images using an aberration corrected Nion UltraSTEM 100 dedicated to advanced STEM imaging, at 100 kV along the [1-10] direction. We apply to this sequence of LR images simple averaging to obtain a Non-Registered Averaged (NRA) image, simple averaging with registration using a rigid method - Vandewalle's (Vandewalle et al., 2006) or rotation calculation and Normalized Cross Correlation for displacement calculation-, to get a Registered Averaged (RA) image, and SR to obtain a HR image with a pixel density two times up the original low resolution images. These three different images, will be compared qualitatively and quantitatively, in terms of SNR and atom column roundness.

To calculate SNR different parallel line profiles have been taken and variations in background, signal and noise have been calculated. To determine the background we apply a Gaussian smoothing kernel with a full-width at half-maximum (FWHM) of two times the average feature between two Fe atoms of double occupancy (Jones & Nellist, 2013). This kernel has been increased in the SR image case in order to maintain the same physical length of FWHM. This background is then subtracted from the original signal to leave a combination of signal and noise. Later, this signal is smoothed again with a narrower Gaussian. By subtracting this smoothed signal and the combination of signal and noise we obtain only the noise. Then the SNR can be expressed as a ratio between the standard deviation of the signal and the standard deviation of the noise.

Atom column roundness constitutes additional interesting quality metric related to the resolving power of HAADF-STEM images. Calculating the roundness value requires recovering the signal of the whole image, then by varying the angle of rotation centred on the maximum intensity peak different radius values can be recorded to generate a profile. In this way, a profile

is generated with all calculated radii providing the atom column shape. Finally, different approaches can be applied to obtain the resulting roundness value. In (Jones & Nellist, 2013), the authors propose a method to demonstrate the relationship between the roundness value and the resolving power when high-frequency noise is reduced. This methodology is based on averaging the width at half maximum height per each profile in every atom column, giving a single number that can also be used in this work as a resolution measure. Then, for a large number of measurements, the roundness value will be lower if the amount of noise is smaller. Consequently, the smaller the roundness value, the higher the resolution.

Additionally, in order to determine other accurate roundness values, in this paper we have also followed the ANSI dimensioning and tolerance standard Y14.5 (Asme 14.5M:, 1994) that defines tolerances of a shape with reference to an ideal geometric feature. Minimum Zone Circle (MZC), the Least Square Circle (LSC) and the Minimum Circumscribed Circle (MCC) (Samuel & Shunmugam, 2003; Simonyan, Grishin, Vatolin, & Popov, 2008; Sui & Zhang, 2012; Xiuming & Jingcai, 2014) have been considered. All these methods calculate the roundness value using different algorithms based on the inner and/or outer circle of atoms from the maximum intensity peak.

3. Results and Discussion

Fig. 2 shows four different Fe_3O_4 images. In first figure (2.a) a LR image belonging to the series acquired experimentally is shown, while in figures 2.b, 2.c and 2.d the corresponding NRA and RA images generated by averaging the experimental series, and the HR image with double pixel density obtained by applying SR are presented. As expected, a reduction of noise is readily observed in these generated images with respect to the LR micrograph, in the interpolated images atomic columns appear less blurred.

The corresponding Fourier Transforms (FT) are shown in figures 3.a, 3.b, 3.c and 3.d

respectively. The existence of irregular oscillations during the 'fly back' time of the probe between successive line scans, it will invariably result in displacements of the rows of pixels (Nadi Braidy et al., 2012; Jones & Nellist, 2013) and the assumption that the electron microscopy image has periodic boundary (Hovden, Jiang, Xin, & Kourkoutis, 2015; Moisan, 2011) produces a cross pattern streaks running vertically and horizontally through the centre of the 2D Fourier transform. For this reason, the images shown in Fig 2 are the FT of "periodic component" of P+S algorithm (Hovden et al., 2015). Accordingly, several Fourier spots can be distinguished with enhanced clarity as result of applying the proposed SR approach (Fig. 3.d), while these spots are hardly visible in the FT of the experimental image (Fig. 3.a), neither in the FT of the NRA and RA images.

This qualitative improvement in the HR image allows appreciating details that are not possible to see in the LR image neither in the corresponding NRA and RA images. Figure 4.a shows a zoomed area of the $Fe_3O_4(111)$ surface of the film using RA image (Fig. 4.a) and its corresponding on the HR image (Fig. 4.b). In this area, and according to the orientation of the material, if top Fe is full monolayer we should see three atom column of Fe, Fe in tetrahedral (Fe_{A1}), in octahedral (Fe_B) and tetrahedral (Fe_{A2}) positions. However, in the RA image we only can clearly distinguish two intensity peaks, the Fe_{A1} and Fe_B (see the surface graph in figure 4.c and a line profile in figure 4.e), whereas in the same area of the HR image where noise has been substantially reduced, the three different Fe atom column positions can be easily identified (surface graph in figure 4.d and line profile in 4.f). This clearly shows that the $Fe_3O_4(111)$ surface consists of full monolayer (Fe_{A1}-Fe_B-Fe_{A2}) of Fe.

The Fe_3O_4 surfaces have been subject on many studies over the years, both experimentally (Barbieri, Weiss, Van Hove, & Somorjai, 1994; Lemire, Meyer, Henrich, Shaikhutdinov, & Freund, 2004; Weiss & Ranke, 2002) and theoretically (Noh, Osman, Aziz, Winget, & Brédas, 2015; Tao et al., 2010; Yu, Huo, Li, Wang, & Jiao, 2012). Recently the (111) surface of

magnetite has attracted a lot of attention as a catalyst for water splitting, hence interest in their atomic and electronic structure. The polar $Fe_3O_4(111)$ surface has been studied by a number of experimental techniques, including LEED, CO adsorption, STM, HREELS, etc. (Barbieri et al., 1994; Lemire et al., 2004; Weiss & Ranke, 2002), as well as theoretically by density functional theory calculations (Noh et al., 2015; Tao et al., 2010; Yu et al., 2012). Depending on the surface preparation sub-monolayer of only Fe_{A1}, 1/3 of monolayer (Fe_{A1}) and 2/3 of monolayer (Fe_{A1}-Fe_B) surface atomic structures were reported. We note that the full monolayer (Fe_{A1}-Fe_B-Fe_{A2}) has been considered only theoretically. Since the full monolayer surface is predicted to be the least stable of surface bulk terminations of $Fe_3O_4(111)$, utilising this surface for variety of heterogeneous reactions that include also water it is of great interest. Finally, we note that models of the most of the experimental techniques are derived by indirect methods with reliability factor (R) being very sensitive to fitting parameters.

Quantitatively, SNR results are shown in Table 1. For the simplest case of a LR image, a SNR value of 2.33 has been obtained. Averaging the series of images results in a significant improvement, around 150%, in the signal to noise ratio (SNR values of 3.51 and 3.58 for NRA and RA images respectively), furthermore we can observe that alignment does not make the difference between both variants of averaging. This value may be lower than the theoretically expected because the original series suffer from distortions parallel and perpendicular to the scan direction and because of the rigid alignment applied.

Finally, SNR calculated for HR image rises to 10,97 dB, a 300% improvement with respect to NRA and RA images and almost a 500% with respect to the corresponding LR SNR, demonstrating a significant quality increase when the proposed SR methodology is applied. This improvement is due to the fact that the reconstruction algorithm used is based on a weighted average of all the pixels with zones of similar intensity, always maintaining the original intensity distribution that allows an analysis of the chemical composition. Whenever

we use a search window of large enough size, we can detect more pixels with similar values of intensity in their neighborhood and therefore increase the number of pixels to average.

Regarding roundness, Table 1 also shows the results comparing the different methods (Jones method, MZC, LSC and MCC). Averaging does not make any remarkable difference against the LR image, even providing higher values in the case of MZC method, that is, the LR image provided a roundness of 0.135 nm, then the averaged images increased up to 0.140 nm, but finally the HR image reduced to 0.119 nm. For Jones and MZC methods, roundness value of LR and NRA images were almost the same, around 0.125 and 0.130 nm respectively, while RA images could reduce this measurement slightly. LSC showed a better result in the NRA image (0.119 nm) with respect to the experimental and the RA images (0.124 and 0.123 nm). However, the best performance was obtained again in the HR images, providing values of 0.115, 0.111 and 0.110 nm. Therefore, roundness measured in the HR image yielded the lowest values whatever the method.

4. Conclusions

Averaging and SR have been applied to a series of ten HAADF-STEM images of Fe_3O_4 (111) in order to improve the resolving power. We have shown through visual inspection in the real and reciprocal space, and by calculations using objective SNR and roundness metrics, that reconstruction methods provide images with less noise and more details than the originals. The registration did not make significant differences in terms of qualitative nor quantitative measurements between both the NRA and RA variants of averaging. Overall the SR outperformed the averaging approximations. The reciprocal space analysis revealed clearly spots in the HR image that were not visible in any other micrograph. By zooming the HR image in the surface region reveals the atomic structure of the surface comprising of full Fe monolayer in tetrahedral, octahedral and tetrahedral positions, respectively. Quality objective measurements of SNR confirmed this improvement, SR yielded values close to five times better

than the LR experimental image signal to noise ratio, and more than three times better than the averaged images. Different measures of roundness have coincided in showing less variability in the shape of the HR atom columns. The proposed SR methodology constitutes a more accurate way of enhancing HAADF-STEM images, allowing the extraction of a larger amount and more accurate information from the series of experimental micrographs. Finally, the application of this method on the cross-sectional HAADF imaging of the Fe_3O_4(111) surface has revealed that the magnetite (111) surface consists of full monolayer of Fe with topmost Fe atoms in tetrahedral position (Fe_{A2}).

References

Asme 14.5M: (1994). Dimensional and Tolerancing Professional Certification. *The American Society of Mechanical ENgineers*, 250.

Barbieri, A., Weiss, W., Van Hove, M. A., & Somorjai, G. A. (1994). Magnetite Fe3O4 (111): surface structure by LEED crystallography and energetics. *Surface Science*, *302*(3), 259–279.

Bárcena-González, G., Guerrero-Lebrero, M. P., Guerrero, E., Fernández-Reyes, D., González, D., Mayoral, A., … Galindo, P. L. (2016). Strain mapping accuracy improvement using super-resolution techniques. *Journal of Microscopy*, *262*(1), 50–58. http://doi.org/10.1111/jmi.12341

Bárcena-González, G., Guerrero-Lebrero, M. P., Guerrero, E., Yañez, A., Fernández-Reyes, D., González, D., & Galindo, P. L. (2017). Evaluation of high-quality image reconstruction techniques applied to high-resolution Z-contrast imaging. *Ultramicroscopy*, *182*, 283–291. http://doi.org/10.1016/j.ultramic.2017.07.014

Berkels, B., Binev, P., Blom, D. A., Dahmen, W., Sharpley, R. C., & Vogt, T. (2014). Optimized imaging using non-rigid registration. *Ultramicroscopy*, *138*, 46–56.

http://doi.org/10.1016/j.ultramic.2013.11.007

Berkels, B., Yankovich, A. B., Shi, F., Voyles, P. M., Dahmen, W., Sharpley, R., & Binev, P. (2012). High Precision STEM Imaging by Non-Rigid Alignment and Averaging of a Series of Short Exposures. *Microscopy and Microanalysis*, *18*(S2), 300–301. http://doi.org/10.1017/S1431927612003352

Binev, P., Blanco-Silva, F., Blom, D., Dahmen, W., Lamby, P., Sharpley, R., & Vogt, T. (2012). High-Quality Image Formation by Nonlocal Means Applied to High-Angle Annular Dark-Field Scanning Transmission Electron Microscopy (HAADF–STEM), 127–145. http://doi.org/10.1007/978-1-4614-2191-7_5

Braidy, N., Le Bouar, Y., Lazar, S., & Ricolleau, C. (2012). Correcting scanning instabilities from images of periodic structures. *Ultramicroscopy*, *118*, 67–76. http://doi.org/10.1016/j.ultramic.2012.04.001

Braidy, N., Le Bouar, Y., Lazar, S., & Ricolleau, C. (2012). Instabilities in scanning probe images of periodic structures: detection and corrections. *Microscopy and Microanalysis*, *18*(S2), 378–379.

Buades, A., Coll, B., & Morel, J. M. (2005). A non-local algorithm for image denoising. *Proceedings of the IEEE Computer Society Conference on Computer Vision and Pattern Recognition*, *2*(0), 60–65. http://doi.org/10.1109/CVPR.2005.38

Hovden, R., Jiang, Y., Xin, H. L., & Kourkoutis, L. F. (2015). Periodic Artifact Reduction in Fourier Transforms of Full Field Atomic Resolution Images. *Microscopy and Microanalysis*, *21*(2), 436–441. http://doi.org/10.1017/S1431927614014639

Jones, L., & Nellist, P. D. (2013). Identifying and correcting scan noise and drift in the scanning transmission electron microscope. *Microscopy and Microanalysis*, *19*(4), 1050–1060. http://doi.org/10.1017/S1431927613001402

Jones, L., Yang, H., Pennycook, T. J., Marshall, M. S. J., Van Aert, S., Browning, N. D., …

Nellist, P. D. (2015). Smart Align—a new tool for robust non-rigid registration of scanning microscope data. *Advanced Structural and Chemical Imaging*, *1*(1), 8. http://doi.org/10.1186/s40679-015-0008-4

Kang, M. G., & Chaudhuri, S. (2003). Super-resolution image reconstruction. *IEEE Signal Processing Magazine*, *20*(3), 19–20. http://doi.org/10.1109/MSP.2003.1203206

Kimoto, K., Asaka, T., Yu, X., Nagai, T., Matsui, Y., & Ishizuka, K. (2010). Local crystal structure analysis with several picometer precision using scanning transmission electron microscopy. *Ultramicroscopy*, *110*(7), 778–782. http://doi.org/10.1016/j.ultramic.2009.11.014

Lemire, C., Meyer, R., Henrich, V. E., Shaikhutdinov, S., & Freund, H.-J. (2004). The surface structure of Fe3O4 (1 1 1) films as studied by CO adsorption. *Surface Science*, *572*(1), 103–114.

Mevenkamp, N., Binev, P., Dahmen, W., Voyles, P. M., Yankovich, A. B., & Berkels, B. (2015). Poisson noise removal from high-resolution STEM images based on periodic block matching. *Advanced Structural and Chemical Imaging*, *1*(1), 3. http://doi.org/10.1186/s40679-015-0004-8

Moisan, L. (2011). Periodic plus smooth image decomposition. *Journal of Mathematical Imaging and Vision*, *39*(2), 161–179. http://doi.org/10.1007/s10851-010-0227-1

Nakanishi, N., Yamazaki, T., Rečnik, A., Čeh, M., Kawasaki, M., Watanabe, K., & Shiojiri, M. (2002). Retrieval process of high-resolution HAADF-STEM images. *Journal of Electron Microscopy*, *51*(6), 383–390. http://doi.org/10.1093/jmicro/51.6.383

Nasrollahi, K., & Moeslund, T. B. (2014). *Super-resolution: A comprehensive survey*. *Machine Vision and Applications* (Vol. 25). http://doi.org/10.1007/s00138-014-0623-4

Noh, J., Osman, O. I., Aziz, S. G., Winget, P., & Brédas, J.-L. (2015). Magnetite Fe3O4 (111) surfaces: Impact of defects on structure, stability, and electronic properties. *Chemistry of*

Materials, *27*(17), 5856–5867.

Ophus, C., Ciston, J., & Nelson, C. T. (2016). Correcting nonlinear drift distortion of scanning probe and scanning transmission electron microscopies from image pairs with orthogonal scan directions. *Ultramicroscopy*, *162*, 1–9. http://doi.org/10.1016/j.ultramic.2015.12.002

Protter, M., Elad, M., Member, S., Takeda, H., & Member, S. (2009). Generalizing the Nonlocal-Means to Super-Resolution Reconstruction. *IEEE Transactions on Image Processing*, *18*(1), 36–51.

Rečnik, A., Möbus, G., & Šturm, S. (2005). IMAGE-WARP: A real-space restoration method for high-resolution STEM images using quantitative HRTEM analysis. *Ultramicroscopy*, *103*(4), 285–301. http://doi.org/10.1016/j.ultramic.2005.01.003

Saito, M., Kimoto, K., Nagai, T., Fukushima, S., Akahoshi, D., Kuwahara, H., … Ishizuka, K. (2009). Local crystal structure analysis with 10-pm accuracy using scanning transmission electron microscopy. *Journal of Electron Microscopy*, *58*(3), 131–136. http://doi.org/10.1093/jmicro/dfn023

Samuel, G. L., & Shunmugam, M. S. (2003). Evaluation of circularity and sphericity from coordinate measurement data. *Journal of Materials Processing Technology*, *139*(1–3 SPEC), 90–95. http://doi.org/10.1016/S0924-0136(03)00187-0

Sang, X., & LeBeau, J. M. (2014). Revolving scanning transmission electron microscopy: Correcting sample drift distortion without prior knowledge. *Ultramicroscopy*, *138*, 28–35. http://doi.org/10.1016/j.ultramic.2013.12.004

Simonyan, K., Grishin, S., Vatolin, D., & Popov, D. (2008). Fast video super-resolution via classification. In *Proceedings - International Conference on Image Processing, ICIP* (pp. 349–352). http://doi.org/10.1109/ICIP.2008.4711763

Sui, W., & Zhang, D. (2012). Four Methods for Roundness Evaluation. *Physics Procedia*, *24*,

2159–2164. http://doi.org/10.1016/j.phpro.2012.02.317

Tao, Y., Wen, X.-D., Jun, R. E. N., Li, Y.-W., Wang, J.-G., & Huo, C.-F. (2010). Surface structures of Fe3O4 (111),(110), and (001): A density functional theory study. *Journal of Fuel Chemistry and Technology*, *38*(1), 121–128.

Vandewalle, P., Süsstrunk, S., & Vetterll, M. (2006). A frequency domain approach to registration of aliased images with application to super-resolution. *Eurasip Journal on Applied Signal Processing*, *2006*, 1–14. http://doi.org/10.1155/ASP/2006/71459

Wang, Y., Suyolcu, Y. E., Salzberger, U., Hahn, K., Srot, V., Sigle, W., & Aken, P. A. Van. (2018). Correcting the linear and nonlinear distortions for atomically resolved STEM spectrum and diffraction imaging, (January), 114–122. http://doi.org/10.1093/jmicro/dfy002

Watanabe, K., Kotaka, Y., Nakanishi, N., Yamazaki, T., Hashimoto, I., & Shiojiri, M. (2002). Deconvolution processing of HAADF STEM images. *Ultramicroscopy*, *92*, 191–199.

Weiss, W., & Ranke, W. (2002). Surface chemistry and catalysis on well-defined epitaxial iron-oxide layers. *Progress in Surface Science*, *70*(1–3), 1–151.

Xiuming, L., & Jingcai, Z. (2014). Evaluation for the minimum circumscribed circle based on the rotation method. *Measurement Science and Technology*, *25*(9), 017002. http://doi.org/10.1088/0957-0233/25/9/097001

Yang, J., & Huang, T. (2010). Image super-resolution: Historical overview and future challenges. *Super-Resolution Imaging*, 3–25.

Yankovich, A. B., Berkels, B., Dahmen, W., Binev, P., & Voyles, P. M. (2015). High-precision scanning transmission electron microscopy at coarse pixel sampling for reduced electron dose. *Advanced Structural and Chemical Imaging*, *1*(1), 2. http://doi.org/10.1186/s40679-015-0003-9

Yu, X., Huo, C.-F., Li, Y.-W., Wang, J., & Jiao, H. (2012). Fe3O4 surface electronic

structures and stability from GGA+ U. *Surface Science*, *606*(9–10), 872–879.

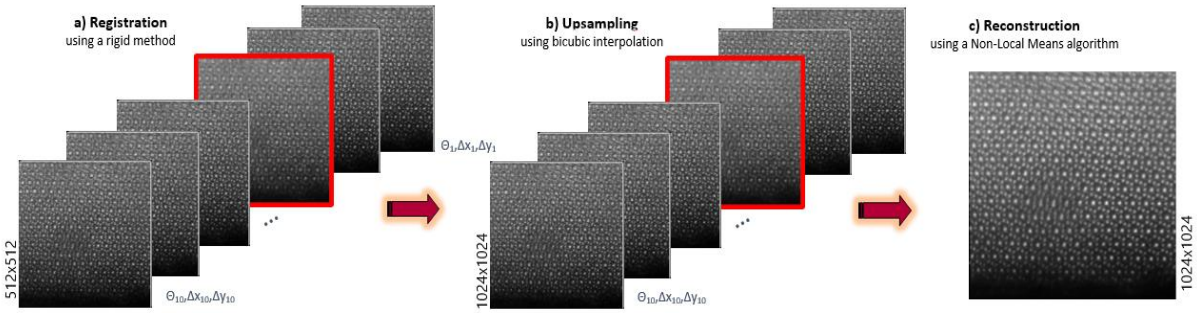

Fig 1. A scheme of the SR methodology. a) Alignment or registration of the image series selecting one of them as reference. b) 2x upsampling using bicubic interpolation. c) Reconstruction using Non-Local Means method.

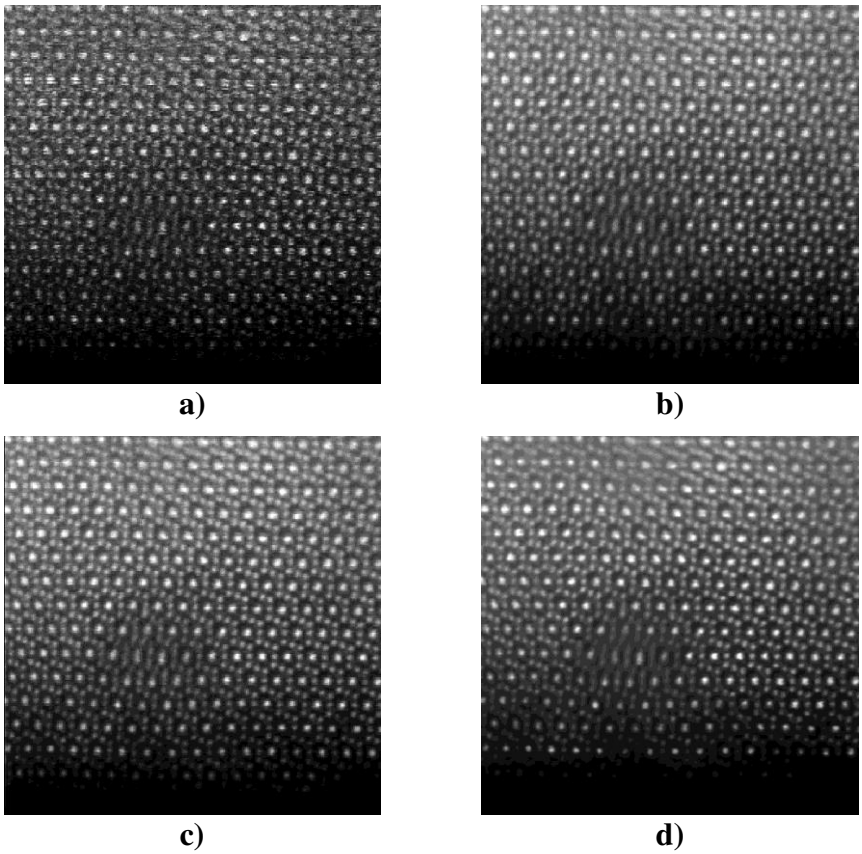

Fig 2. HAADF-STEM of Fe_3O_4 along the [1-10] zone axis. a) Fist image of a series of 10 images experimentally acquired. b) NRA Image, resulting from averaging the experimental series without previous registration. c) RA Image, resulting from aligning and averaging the experimental series. d) HR image applying SR.

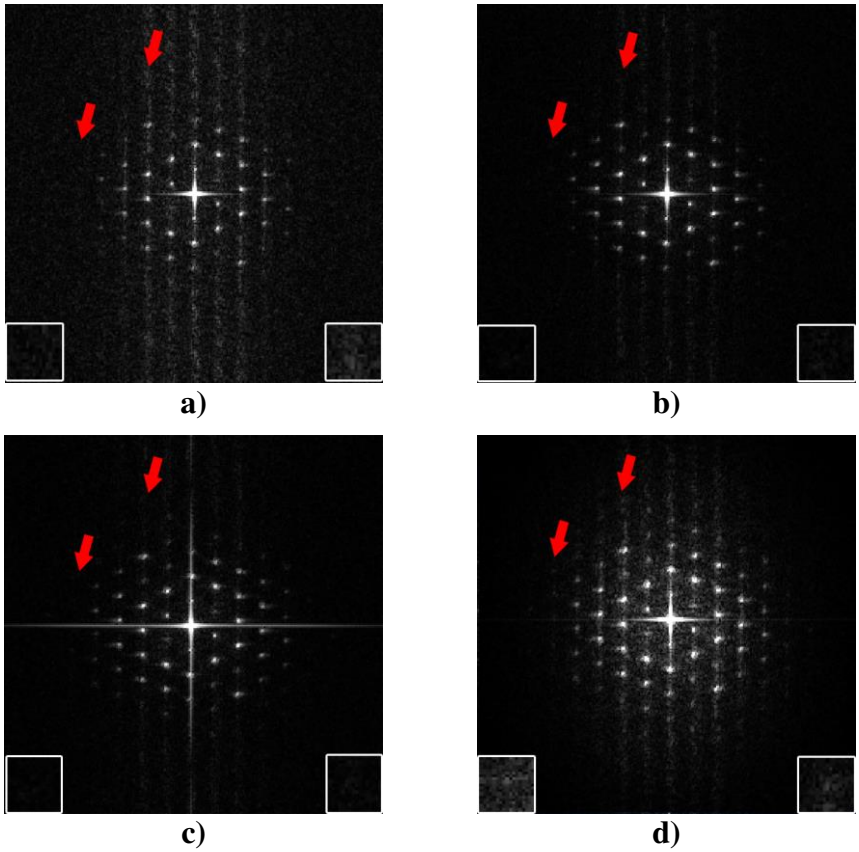

Fig 3. Fourier Transforms of the a) LR image, b) NRA image, c) RA image and d) HR image. The squares in each image correspond to two particular spots (pointed with the red arrows) that have been zoomed to try to appreciate more details. These selected spots can be clearly appreciated in the FT of the HR image.

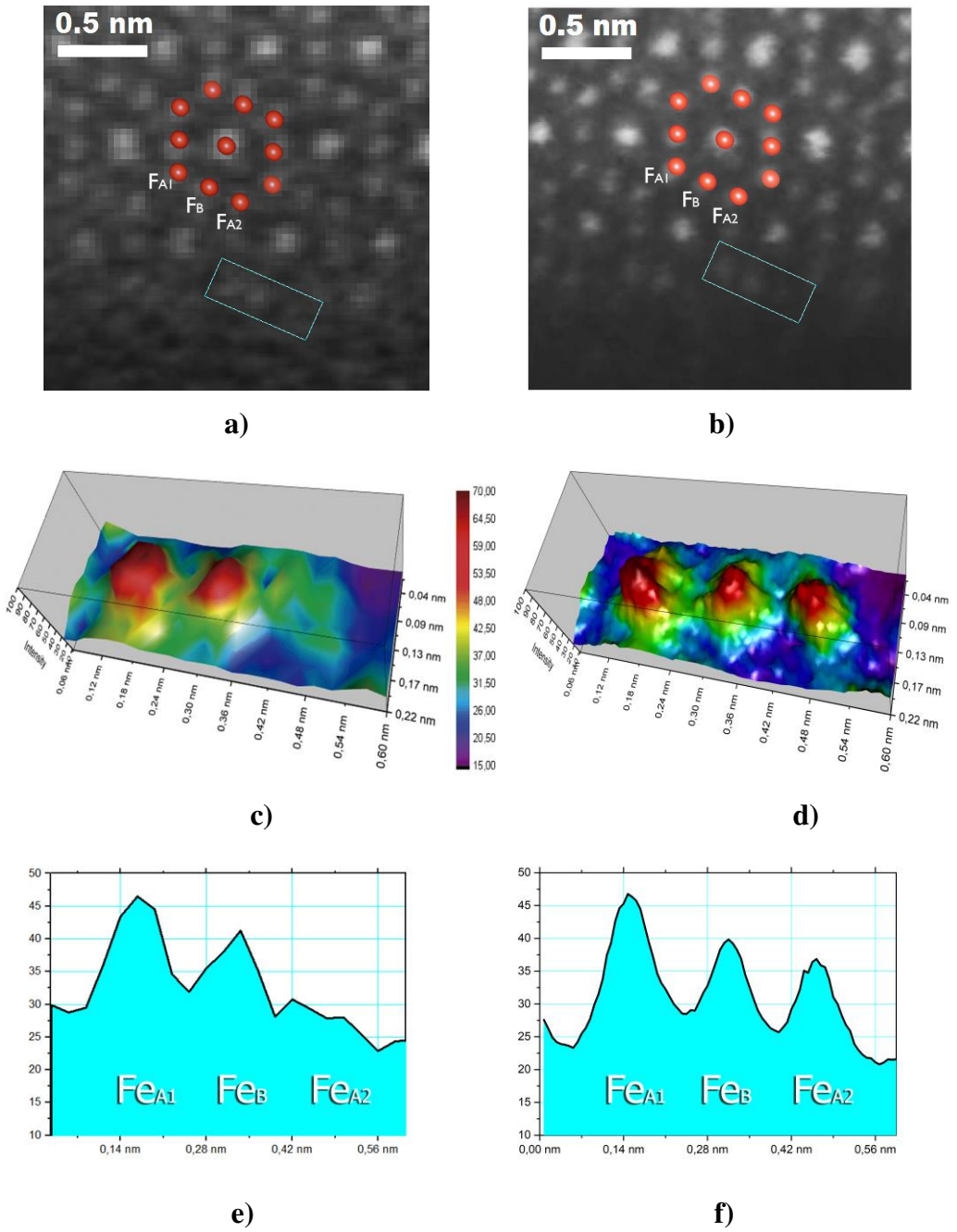

Fig 4. a) Zoomed area of the surface region of $Fe_3O_4(111)$ surface region in the RA image and b) the same zoomed area in the HR image. –. Fe_{A1} and Fe_B denotes the Fe atom columns in tetrahedral and octahedral positions, respectively. a) and b) have been saturated in order to highlight the difference between both images. c) and d) represents the corresponding surface graphs while e) and f) the intensity profiles corresponding to the rectangular area indicated in a) and b). In e) two of the three intensity peaks can be observed while the three atom columns of Fe in different occupation sites can be clearly identified in f).

	Signal-Noise Ratio (db)	Roundness (nm)			
		Jones Method	Minimum Zone Circle (MZC)	Least Square Circle (LSC)	Minimum Circumscribed Circle (MCC)
Low resolution image (LR)	2.33	0.125	0.135	0.124	0.130
Non-Registration Averaged image (NRA)	3.51	0.126	0.140	0.119	0.130
Registration Averaged image (RA)	3.58	0.123	0.139	0.123	0.128
High-Resolution image (HR)	10.97	0.110	0.119	0.111	0.115

TABLE 1. Comparative table with SNR and Roundness values for average resolution and MZC, LSC and MCC algorithms.